JOURNAL OF MATERIALS SCIENCE 29 (1994) 3441–3450

Phase composition and mechanism of formation of Ba–β-alumina-type systems for catalytic combustion prepared by precipitation

G. GROPPI, C. CRISTIANI, P. FORZATTI*
Dipartimento di Chimica Industriale e Ingegneria Chimica "G. Natta" del Politecnico, P. za Leonardo da Vinci 32, I-20133 Milano, Italy

M. BELLOTTO
CISE, P.O. Box 12081, 20134 Segrate Milano, Italy

A novel preparation method is proposed for Ba–β-Al_2O_3-type systems to be used in high-temperature catalytic combustion, consisting of precipitation in aqueous medium. Differential thermal analysis–thermogravimetry, X-ray diffraction, Fourier transform-infrared, TEM and surface area data are presented for Ba–Al-O samples with Al/Ba atomic ratios in the range 14–9 calcined at different temperatures up to 1670 K. The final materials consist of a barium-poor Ba–β_I-Al_2O_3 phase together with 1% α-Al_2O_3 in the case of Al/Ba = 14 and of a barium-rich Ba–β_{II}-Al_2O_3 phase together with 2% $BaAl_2O_4$ in the case of Al/Ba = 9. A monophasic sample with a Ba–β-Al_2O_3 structure is obtained in the case of Al/Ba = 12; this phase is constituted by the simultaneous presence of both β_I and β_{II} structure types. Two routes operate above 1370 K in the formation of the Ba–β-Al_2O_3 phases involving solid-state reactions between γ-Al_2O_3 and $BaAl_2O_4$, and γ-Al_2O_3 and dispersed barium compounds. Based on the analogies between the structures of γ-Al_2O_3 and of the Ba–β-Al_2O_3 phases it is suggested that the formation of the latter occurs via diffusion of barium ions within oxygen close-packed planes of the γ-Al_2O_3-type spinel structure.

1. Introduction

Catalytic combustion is currently considered to be a promising method for the effective combustion of lean fuel–air mixtures in gas turbines with minimum emission of NO_x, CO and unburned hydrocarbons.

In view of the extreme operating conditions of the combustor ($T = 1470$–1570 K, $P = 10$–15 atm, $v = 10$–40 m s^{-1}), catalytic materials with high thermal stability and high resistance to thermal shocks are needed for the development of this technology [1–3]. Among the investigated systems Ba–Al oxide-based catalysts appear to be promising materials due to their excellent thermal stability. Machida *et al.* [4, 5] attributed the thermal stability of these materials to the formation of barium hexa-aluminate ($BaO \cdot 6Al_2O_3$) and they observed that a large surface area (10–15 m^{2}g^{-1}) is obtained upon calcination at 1570 K using a preparation method based on the hydrolysis of the corresponding alkoxides in an organic medium. According to the phase diagram of the Ba–Al–O system [6], the $BaO \cdot 6Al_2O_3$ phase is stable up to its melting point of 2190 K. The high thermal resistance to sintering has been related to the layered β-Al_2O_3-type structure of barium hexa-aluminate, consisting of spinel blocks of $[Al_{11}O_{16}]^+$ separated by mirror planes where the large barium cations are located [7]. This structure is expected to suppress interlayer diffusion of atoms and crystal growth along the *c*-axis (perpendicular to the mirror plane). This eventually accounts for the plate-like shape of the crystallites, as revealed by TEM measurements. It was reported that the alkoxide preparation route ensures interspersion of the constituents in the precursor at the molecular level, so that the formation of the $BaO \cdot 6Al_2O_3$ phase does not occur by diffusion-controlled solid-state reaction but by direct transformation of the amorphous precursor without the formation of intermediates. The final material shows a β-Al_2O_3-type structure and good morphological properties. Barium hexa-aluminate has also been prepared starting from powder mixtures of $BaCO_3$ and γ-Al_2O_3 [4]. In this case, $BaAl_2O_4$ forms as an intermediate product, $BaO \cdot 6Al_2O_3$ is obtained via solid-state reaction between γ-Al_2O_3 and $BaAl_2O_4$ and the final material shows a low surface area ($S_a \cong 5$ m^{2}g^{-1}). It was suggested that high surface areas are prevented by the growth of $BaAl_2O_4$ particles during the diffusion-controlled solid-state reaction to give $BaO \cdot 6Al_2O_3$.

*Author to whom all correspondence should be addressed.

0022–2461

The alkoxide method also allows the incorporation of transition metal ions into the structure of the final material as active elements for catalytic combustion [8]. Accordingly, the catalyst can be directly prepared by extrusion in the monolith form that is required for power applications.

Although the $BaO \cdot 6Al_2O_3$ system has been described as a monophasic compound with structure related to that of β-Al_2O_3, it is now well established that this compound is actually constituted by two distinct phases, β_I and β_{II}, with composition $BaAl_{14.66}O_{23}$ and $BaAl_{9.15}O_{14.73}$, respectively [9, 10]. Accordingly, materials with the β-Al_2O_3-type structure could be obtained in the range 14.6–9.1 of the Al/Ba ratio.

In a previous paper [11], we reported an alternative preparation method based on the precipitation of the constituents by $(NH_4)_2CO_3$ from an aqueous solution of the corresponding nitrates. According to this route, $BaMn_xAl_{12-x}O_{19}$ systems ($x = 0$, 1, 2) with structural, morphological and catalytic properties close to those reported for the samples prepared via the alkoxide route, have been obtained. In the present work, the same method has been used to prepare samples with Al/Ba atomic ratios ranging from 14–9. The thermal evolution of the samples has been investigated by X-ray diffraction (XRD), Fourier transform–infrared spectroscopy (FT–IR), surface area and transmission electron microscopy (TEM) measurements with the aim to clarify the phase composition and the morphological properties as a function of the Al/Ba atomic ratio. The formation mechanism of the final material with the β-Al_2O_3-type structure is also addressed. Finally, the peculiarities of the proposed preparation method in the development of the structural and morphological properties of the final material are discussed.

2. Experimental procedure

2.1. Preparation of the samples

Ba–Al–O samples with Al/Ba = 14, 12, and 9 were prepared by precipitation in aqueous medium [11]. $Ba(NO_3)_2$ (Fluka 99%) was completely dissolved in hot water ($T = 330$ K) under vigorous stirring. The resulting solution was acidified (pH $\approx$ 1) with HNO_3 and then Al $(NO_3)_3 \cdot 9H_2O$ (Fluka 98%) was added. The solution containing barium and aluminium ions was poured under vigorous stirring into a solution of $(NH_4)_2CO_3$ at constant temperature ($T = 330$ K), and the formation of a white precipitate was observed. The slurry was then aged at 330 K for about 3 h; the pH of the slurry varied in the range 7.5–8. The precipitate was filtered, washed and dried at 380 K overnight. Analysis by atomic absorption for barium and aluminium contents in mother liquors and washing waters indicated that the precipitation occurred in a quantitative way. Chemical analysis of the dried samples confirmed that the actual Al/Ba ratios correspond to the nominal ones.

Al_2O_3, $BaCO_3$ and $BaAl_2O_4$ were prepared as reference compounds according to the same procedure.

2.2. Characterization of samples

The precursor was dried at 380 K, ground between 150–200 mesh and then calcined at different temperatures (470, 770, 970, 1170, 1270, 1370, 1470, 1570, and 1670 K) according to the following calcination procedures: heating rate 60 K h^{-1}, holding 10 h, cooling rate 100 K h^{-1}. No grinding of the samples was performed after each calcination.

The samples were characterized by means of different physico-chemical techniques.

XRD analyses were performed by a Philips PW 1050–70 vertical goniometer using a nickel-filtered CuK_α radiation. Crystallite dimensions were calculated using the Scherrer equation [12]. The amount of $BaAl_2O_4$ was determined by quantitative XRD analysis; the calibration curve was obtained using γ-Al_2O_3 and $BaAl_2O_4$ mixtures in different weight percentages [12]. The (2 0 2) reflection of $BaAl_2O_4$ was used for this purpose, and its intensity was measured according to a profile-fitting procedure [13].

FT–IR spectra were recorded on a Perkin–Elmer 1720 Spectrophotometer, using the KBr pressed-disc technique. Surface areas were determined by nitrogen absorption with the BET method using a Carlo Erba Sorptomatic 1900 series. Differential thermal–thermogravimetric (DTA–TG) analyses in air up to 1270 K (heating rate 10 K min^{-1}) were accomplished using a SETARAM 100–200 instrument. TEM measurements were performed using a Jeol JEM 200CX instrument.

In this paper the Ba–Al–O samples are quoted according to the Al/Ba atomic ratio and the calcination temperatures: e.g. Ba1Al14–1470 indicates a sample with an atomic ratio Al/Ba = 14 and calcined at 1470 K.

3. Results

3.1. Dried samples

The samples dried at 380 K represent the matrices from which all subsequent samples have been derived. The XRD powder pattern of Al_2O_3–380 (Fig. 1a) shows the reflections attributed to $(NH_4)_2Al_6(OH)_{14}(CO_3)_3 \cdot H_2O$ (AACHH) [14]. No other reflections can be detected. The reflections of this phase are also evident in the XRD spectra of Ba1Al14–380, Ba1Al12–380, and Ba1Al9–380 (Fig. 1b–1d). Other reflections are present in these samples that can be tentatively attributed to mixed Ba–Al compounds, namely $BaAl_2(CO_3)_2(OH)_4 \cdot 2H_2O$ (JCPDS 31–116) and $Ba_2Al_4(OH)_{16}$ (JCPDS 24–16). As expected, the intensities of the main peaks of $BaAl_2(CO_3)_2(OH_4) \cdot 2H_2O$ ($2\theta = 9.85°$) and of $Ba_2Al_4(OH)_{16}$ ($2\theta = 18.50°$) decrease on increasing the Al/Ba ratio. The FT–IR spectra of Al_2O_3–380 and of Ba1Al14–380, Ba1Al12–380, and Ba1A19–380 show the bands of CO_3^{2-} species (in the regions 800–1050 and 1200–1400 cm^{-1}) and of NH_4^+ species (bands at 1410 and 3180 cm^{-1}). These results are in line with the XRD data; however, a contribution to these bands from amorphous compounds cannot be excluded.

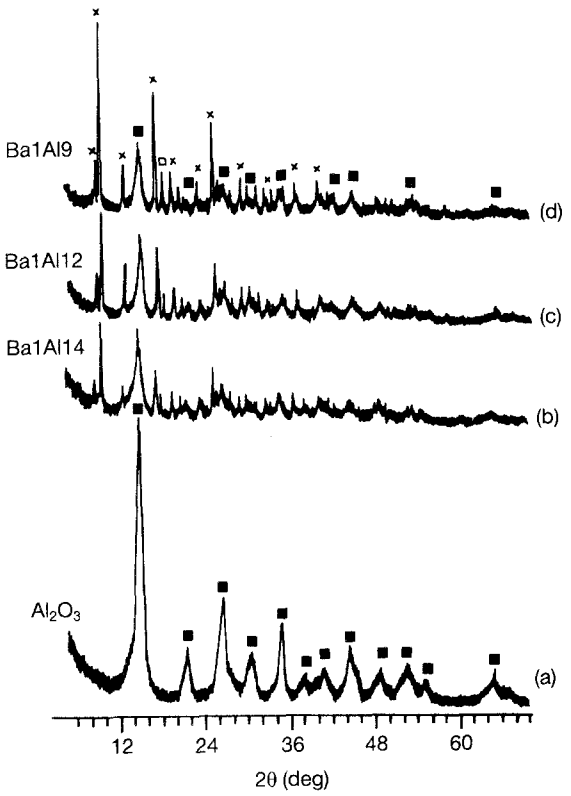

Figure 1 XRD spectra of (a) Al_2O_3, (b) Ba1Al14, (c) Ba1Al12 and (d) Ba1Al9 dried at 380 K overnight. AACHH: (■) $(NH_4)_2Al_6(OH)_{14}(CO_3)_3 \cdot H_2O$. (×) $BaAl_2(CO_3)_2(OH)_4 \cdot 2H_2O$, (□) $BaAl_4(OH)_{16}$.

3.2 Thermal evolution of the precursors up to 1270 K

The DTA–TG curves in air of Al_2O_3–380, Ba1Al14–380, Ba1Al12–380, and Ba1Al9–380 up to 1270 K (Fig. 2) show the following common features: (i) an endothermic peak with maximum at T=410–430 K and weight loss≈5%; (ii) an endothermic peak starting from 440 K and with maximum at $T \approx 530$ K and weight loss≈30%–35%; (iii) a couple of endothermic peaks in the range 620–740 K with an associated weight loss of ≈5%. The above temperatures and the related thermal effects compare well with those reported in the literature for the decomposition of AACHH to pseudobohemite (T_{max}=410–430 K and 530 K, overall weight loss 38%) [14] and the consecutive transition pseudobohemite →γ-Al_2O_3 (T_{max} = 650–720 K) [15]. In the barium-containing samples, in addition to the above effects, a small endothermic peak at $T \approx 1190$ K with weight loss≈ 1%–2% is clearly evident when an expanded scale is used. This peak can be tentatively associated with the formation of $BaAl_2O_4$ in line with the XRD evidence as described below.

The XRD spectra of Al_2O_3–470 and of the Ba1AlX–470 samples (Fig. 3) confirm that the AACHH crystalline phase, present in the precursors, decomposes upon calcination at 470 K to give a microcrystalline pseudobohemite phase. In the barium-containing samples too, the characteristic reflections of the crystalline barium phases disappear and only small amounts of microcrystalline $BaCO_3$ (Witherite (JCPDS 5-378)) are present (Fig. 3b–d). In line with XRD and DTA–TG results, the FT–IR spectra

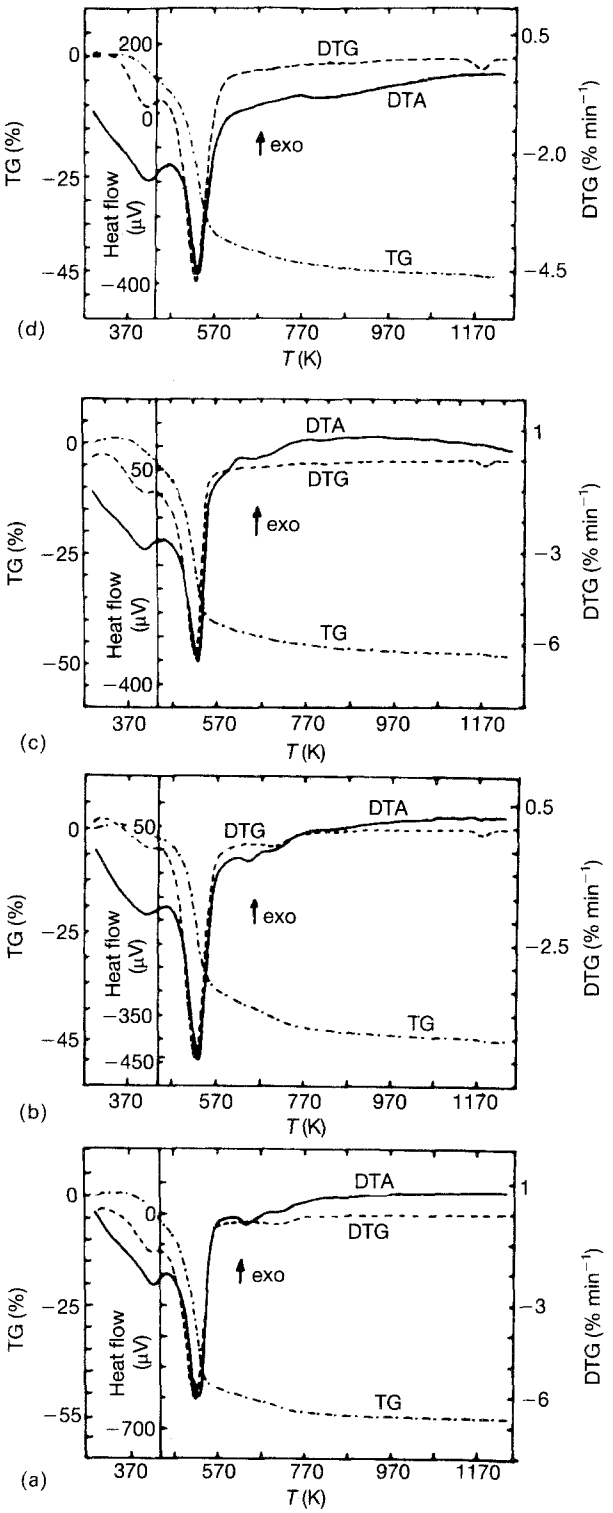

Figure 2 DTA–TG up to 1270 K (heating rate 10 K min^{-1}) in air of (a) Al_2O_3, (b) Ba1Al14, (c) Ba1Al12 and (d) Ba1Al9 dried at 380 K overnight.

show the disappearance of the bands at 1410 and 3180 cm^{-1}, associated with NH_4^+ species and the appearance of new bands at 500, 610, 720, 1065 and 1160 cm^{-1}, associated with the pseudobohemite phase. In addition, the FT–IR spectra show the presence of strong bands in the spectral region 800–850 and 1400–1600 cm^{-1} related to CO_3^{2-} species.

Calcination of all the samples at 770 K results in the transition of pseudobohemite to microcrystalline γ-Al_2O_3, as indicated by the disappearance of the peaks of the former phase and by the appearance of the modulations of the latter phase (JCPDS 10-425) in the

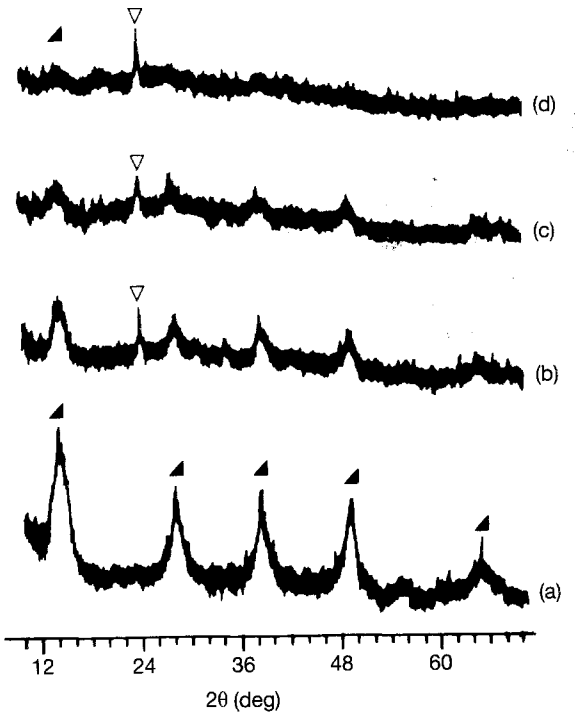

Figure 3 XRD spectra of (a) Al_2O_3, (b) Ba1Al14, (c) Ba1Al12 and (d) Ba1Al9 calcined at 470 K for 10 h. (▲) Pseudobohemite, (▽) $BaCO_3$.

XRD spectra (Fig. 4). These results are consistent with DTA–TG analysis (endothermic peaks at $T = 650$–720 K associated with the pseudobohemite $\rightarrow \gamma$-Al_2O_3 transition) and with the FT–IR results where the formation of γ-Al_2O_3 phase is revealed by the presence of bands at 500 and 800 cm^{-1}. The reflections of $BaCO_3$ are no longer present in the XRD spectra, while the bands of CO_3^{2-} species, likely related to amorphous barium compounds are still evident in the FT–IR spectra.

No changes in the phase composition of Ba1AlX samples are observed upon calcination at 970 K.

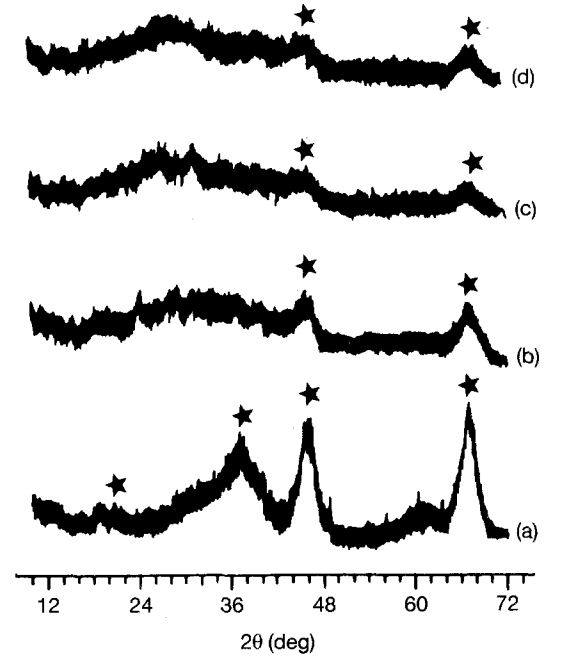

Figure 4 XRD spectra of (a) Al_2O_3, (b) Ba1Al14, (c) Ba1Al12 and (d) Ba1Al9 calcined at 770 K for 10 h. (★) γ-Al_2O_3.

Worthy of note is that γ-Al_2O_3 in the pure system is more crystalline than in the case of Ba–Al–O samples: a mean crystallite dimension of 4.5 nm was calculated for pure Al_2O_3, while no crystallite dimensions could be determined for the barium-containing samples due to the diffusiveness of the reflections.

Calcination at 1170 K induces the formation of crystalline $BaAl_2O_4$ ($d \approx 47$ nm) for all Ba–Al–O samples. In addition, FT–IR measurements furnish evidence of the presence of amorphous carbonates. Noticeably upon calcination at this temperature, γ-Al_2O_3 partially transforms into θ-Al_2O_3 in the case of pure Al_2O_3, while this transition is not observed in the case of barium-containing samples. The above effects are confirmed and are more evident in the samples calcined at 1270 K. Indeed, detailed inspection of the XRD spectra (Fig. 5) indicates the presence only of θ-Al_2O_3 (JCPDS 35-121) with $d_{cryst} \approx 10$ nm in the case of the Al_2O_3 sample, and of microcrystalline γ-Al_2O_3 and crystalline $BaAl_2O_4$ in the case of barium-containing samples. In addition, the FT–IR spectra still provide evidence for the presence of amorphous carbonate species.

In Fig. 6 the surface areas of the samples are plotted as a function of calcination temperature in the range 380–1270 K. All samples have a high surface area at 380 K. For all the investigated samples the surface area increases upon calcination at 470 K due to the decomposition of the thermally unstable crystalline compounds into microcrystalline or amorphous

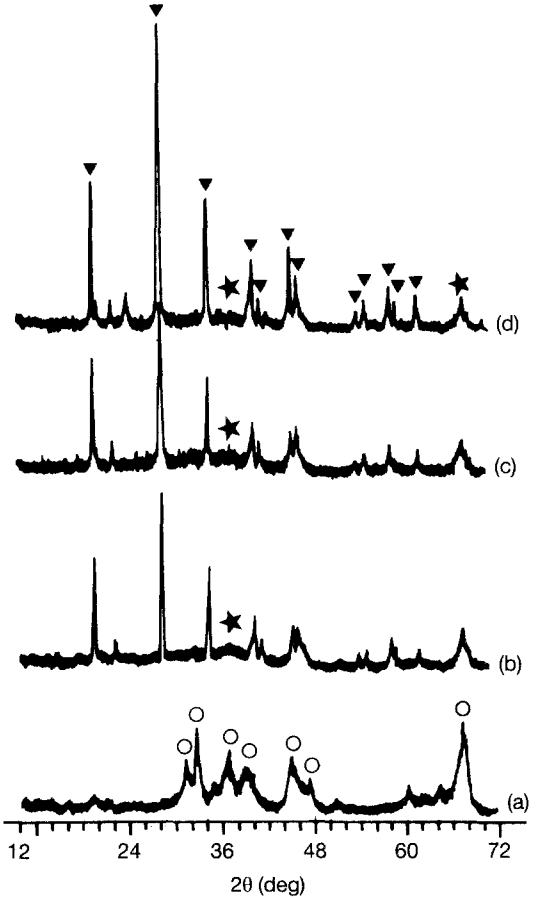

Figure 5 XRD spectra of (a) Al_2O_3, (b) Ba1Al14, (c) Ba1Al12 and (d) Ba1Al9 calcined at 1270 K for 10 h. (★) γ-Al_2O_3, (○) θ-Al_2O_3, (▾) $BaAl_2O_4$.

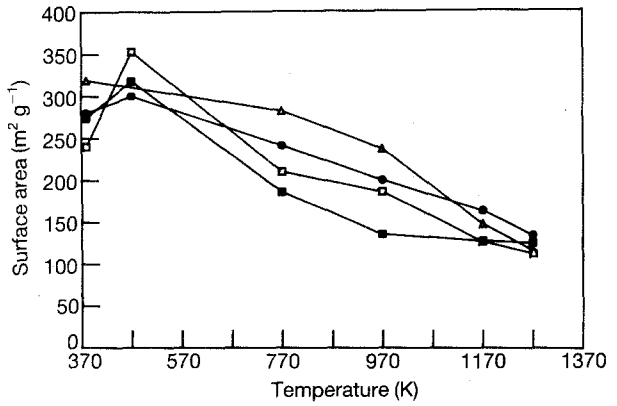

Figure 6 Surface areas of (△) Al_2O_3, (●) BaIAl14, (□) BaIAl12 and (■) BaIAl9 calcined in the temperature range 380–1270 K.

phases and then slowly decreases due to the transformation of pseudobohemite into γ-Al_2O_3 and to the initial sintering of the materials. A tendency for a slightly faster sintering process is apparent in the case of pure alumina above 970 K, where the γ-$Al_2O_3 \rightarrow$ θ-Al_2O_3 transition occurred. In accordance with the low crystallinity of the samples, high surface areas, about 100–120 $m^2 g^{-1}$, are measured even up to 1270 K.

3.3. Formation of the final materials

Upon calcination at 1370 K the incipient formation of Ba–β-Al_2O_3 phase is observed for all the barium-containing samples. In the XRD spectra (Fig. 7b–d) the characteristic reflections of this phase are present, together with those of γ-Al_2O_3 and $BaAl_2O_4$, whereas the transitions of γ-Al_2O_3 to θ-Al_2O_3 and α-Al_2O_3 are not observed. Residual amounts of amorphous carbonates are still evident in the FT–IR spectra. On the other hand, in the case of the Al_2O_3 sample, the XRD data (Fig. 7a) show that θ-Al_2O_3 is partially transformed into α-Al_2O_3 (JCPDS10-173), in line with literature indications [16]. Mean crystallite dimensions of $\approx$20 and $\approx$45 nm are measured for θ-Al_2O_3 and α-Al_2O_3, respectively.

In order to quantify to what extent $BaAl_2O_4$ accounts for the overall barium content, quantitative XRD analyses were performed on the samples calcined at 1170 K–1670 K for 10 h. As shown in Fig. 8 the relative amount of crystalline $BaAl_2O_4$ increases with the nominal barium content and reaches a maximum in the samples calcined at 1270 K. Nevertheless, even at this temperature, $BaAl_2O_4$ accounts only for 40%–65% of the overall barium content and its amount does not increase with further calcination at this temperature (from 5 to 25 h). This behaviour eventually indicates that the reactions responsible for the formation of $BaAl_2O_4$ are not limited by the kinetics but rather by the availability of reactive barium atoms.

The XRD data indicate that the formation of the Ba–β-Al_2O_3 phase is favoured on increasing the calcination temperature above 1370 K and is accompanied by the decrease of $BaAl_2O_4$. In fact, in the XRD spectra of BaIAl14–1470 and BaIAl12–1470

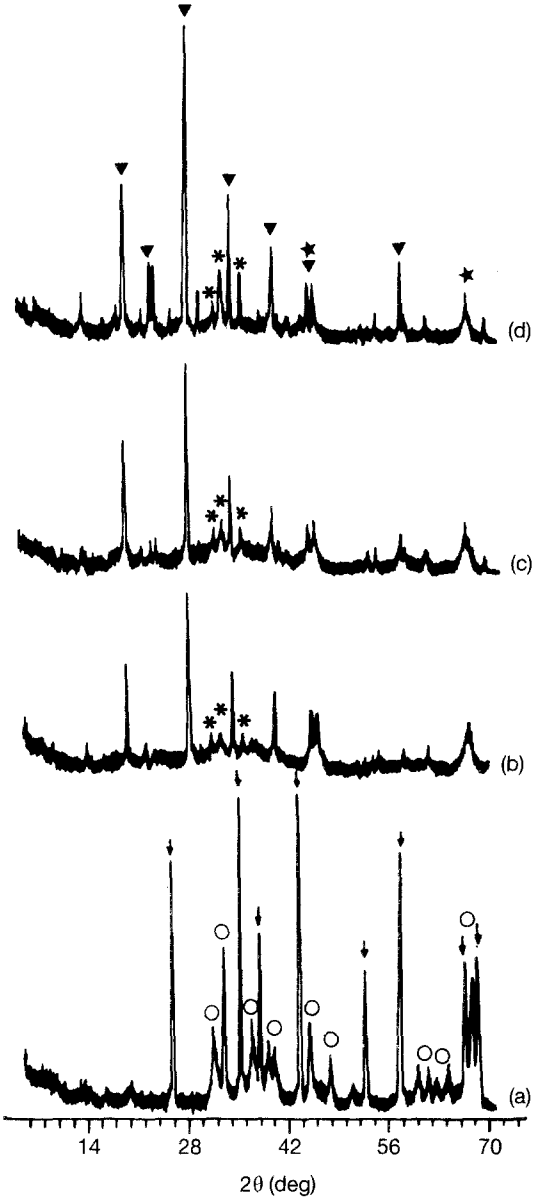

Figure 7 XRD spectra of (a) Al_2O_3, (b) BaIAl14, (c) BaIAl12 and (d) BaIAl9 calcined at 1370 K for 10 h. (★) γ-Al_2O_3, (↓) α-Al_2O_3, (∗) β-Al_2O_3, (○) θ-Al_2O_3, (▾) $BaAl_2O_4$.

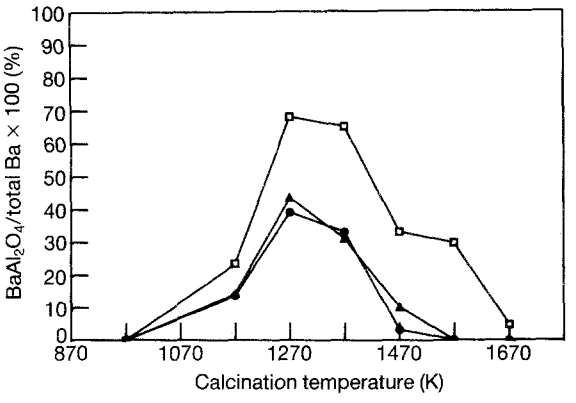

Figure 8 Relative percentage amount of barium segregated as crystalline $BaAl_2O_4$ in samples (△) BaIAl14, (●) BaIAl12 and (□) BaIAl9 versus calcination temperature.

(Fig. 9b–c), only minor amounts of crystalline $BaAl_2O_4$ are detected, while in BaIAl9–1470 (Fig. 9d) a significant amount of this phase is still present. All the other reflections present in the spectra of these

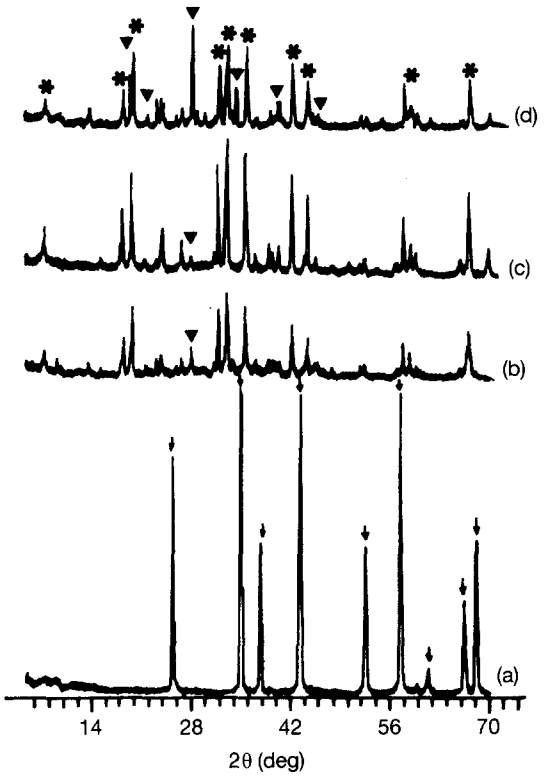

Figure 9 XRD spectra of (a) Al_2O_3, (b) BaIAl14, (c) BaIAl12 and (d) BaIAl9 calcined at 1470 K for 10 h. (↓) α-Al_2O_3, (*) β-Al_2O_3, (▾) $BaAl_2O_4$.

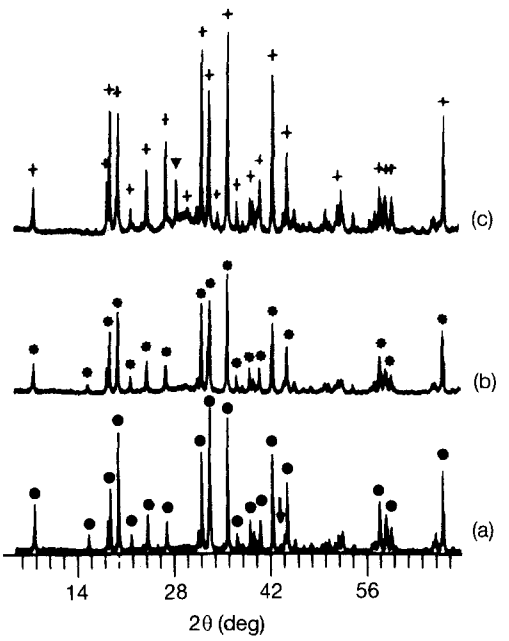

Figure 10 XRD spectra of (a) Al_2O_3, (b) BaIAl14, (c) BaIAl12 and (d) BaIAl9 calcined at 1670 K for 10 h. (*) Ba–$\beta_I\beta_{II}$-Al_2O_3, (▾) $BaAl_2O_3$, (●) Ba–β_I-Al_2O_3, (+) Ba–β_{II}-Al_2O_3, (↓) α-Al_2O_3.

samples can be attributed to a β-Al_2O_3 phase. At this temperature the characteristic FT–IR bands of carbonates species are detected only in the case of BaIAl9. After calcination at 1570 and 1670 K, the XRD reflections of $BaAl_2O_4$ completely disappear in the case of BaIAl14 and BaIAl12 samples, while they are still present in the case of BaIAl9 (Fig. 10). The Ba–β-Al_2O_3 phase is stable for all the Ba–Al–O samples up to 1670 K. The relative intensities of the peaks of this phase in the range 30°–37° 2θ and in the range 15°–21° 2θ change with the Al/Ba ratio. This eventually suggests the presence of differences in the structure of the β-Al_2O_3 phase depending on the barium content of the samples, and in line with the literature [9, 10]. It is worthy, of note that the pure Al_2O_3 samples upon calcination above 1370 K always consist of well-crystallized α-Al_2O_3 (Fig. 9a), whereas α-Al_2O_3 is observed only in very small amounts in BaIAl14–1670.

The phase composition and the crystal structure of the Ba–Al–O samples calcined at 1670 K have been investigated in detail by Rietveld analysis of the XRD powder data [17]. The results of this study are summarized in Table I. In line with literature indications for single-crystal materials, the analysis confirmed that two different β phases, namely β_I and β_{II}, have been formed depending on the Al/Ba ratio. Both phases are made of layered structures of γ-Al_2O_3-related spinel blocks $[Al_{11}O_{16}]^+$ separated by planes containing barium ions. The structures of both phases contain defective and non-defective cells. In the case of β_I the non-defective cell of formula $[Ba_2O_2Al_{22}O_{32}]^{2+}$ consists of two spinel blocks and two barium planes, while the defective cell of formula $[O_4Al_{22}O_{32}]^{6-}$ originates from the presence of barium vacancies ions inducing complex defect structures. To maintain electroneutrality, three non-defective cells are present for each defective one, resulting in an overall theoretical composition of $BaAl_{14.67}O_{23}$. The β_{II} phase also consists of the same non-defective β_I cell and of defective cells of composition $[Ba_3Al_{20}O_{35}]^{4-}$ where barium ions are allocated also into the spinel blocks. To ensure electroneutrality, two non-defective cells are present for each defective one, resulting in an overall theoretical composition of $BaAl_{9.15}O_{14.73}$. In the case of Ba–β_{II}-Al_2O_3, it has been reported [18] that a superstructure $a3^{1/2} \times a3^{1/2}$,

TABLE I Results of Rietveld analysis

Sample	Phase	Composition of β-Al_2O_3	Cell parameters	
			a_0 (nm)	c_0 (nm)
BaIAl14	Ba–β_I-Al_2O_3 2% α-Al_2O_3	$BaAl_{15.34}O_{24.10}$	0.558 76 (2)	2.272 70 (9)
BaIAl12	Ba–$\beta_I\beta_{II}$-Al_2O_3	$BaAl_{12.07}O_{20.11}$	0.559 36 (4)	2.276 7 (2)
BaIAl9	Ba–β_{II}-Al_2O_3 2% $BaAl_2O_4$	$BaAl_{9.23}O_{14.82}$	0.560 16 (3)	2.290 5 (1)

disordered along the c-axis, formed and it is revealed by the appearance of a hump in the XRD spectra in the region of $2\theta = 28°–30°$.

Results of Rietveld analysis on BaIAl14–1670 indicated that this sample consists of a Ba–β_I-Al_2O_3 phase with calculated Al/Ba = 15.34 and cell parameters $a_0 = b_0 = 0.55876(2)$ nm, $c_0 = 2.272\,70(9)$ nm that compare well with those reported in the literature ($a_0 = b_0 = 0.558\,7(2)$ nm and $c_0 = 2.272\,7(1)$ nm [19]). In the case of BaIAl9–1670 Rietveld analysis indicated the presence of the Ba–β_{II}-Al_2O_3 phase with calculated Al/Ba = 9.23 and cell parameters $a_0 = b_0 = 0.560\,16(3)$ nm $c_0 = 2.290\,5(1)$ nm that compare well with those reported in the literature ($a_0 = b_0 = 0.560\,03(5)$ nm and $c_0 = 2.292\,2(2)$ nm [18]. The β_{II} nature of the BaIAl9–1670 sample is confirmed by the appearance of a hump in the region of $2\theta = 28°–30°$ (see Fig. 10c). Results from Rietveld analysis performed on sample BaIAl12–1670 show that the structure of the Ba–β-Al_2O_3 phase in this sample is constituted by the simultaneous presence of both β_I and β_{II} structure types, and is characterized by calculated cell parameters $a_0 = b_0 = 0.559\,36(4)$ nm and $c_0 = 2.276\,7(2)$ nm, that are intermediate between those of phase β_I and β_{II}. These data are in line with previous literature indications [20]. The composition of the Ba–β-Al_2O_3 phase was found to account for the overall chemical composition of the sample ($(Al/Ba)_{calc} = 12.7$ compared to $(Al/Ba)_{th} = 12$). Also, in this case, the presence of the hump in the region $2\theta = 28°–30°$ of the XRD spectrum, less intense than that observed in the BaIAl9–1670 sample, confirms the partial β_{II} nature of BaIAl12–1670. TEM analysis performed on the BaAl12–1670 sample also indicates the presence of hexagonal plate-like crystallites characterized by a strong anisotropy along the (0 0 1) direction.

In Fig. 11 the surface areas of the samples are plotted as a function of calcination temperature for $T \geqslant 1270$ K. High surface areas of the order of $\sim 100\ m^2\,g^{-1}$ are retained in the case of the barium-containing samples upon calcination at 1370 K, whereas a significant decrease in surface area is observed in the case of Al_2O_3 ($S_{a,Al-1370} = 50\ m^2\,g^{-1}$) due to the partial transition of θ-Al_2O_3 into α-Al_2O_3. For all the samples a drop in the surface area upon calcination at $T = 1470$ K parallels the formation of Ba–β-Al_2O_3 phase in the case of barium containing samples and of α-Al_2O_3 in the case of pure Al_2O_3. The higher values measured at 1470 K for Ba–Al–O systems ($\approx 15–30\ m^2\,g^{-1}$) than for Al_2O_3 are probably associated with the layered structure of Ba–β-Al_2O_3 that is expected to suppress crystal growth along the c-axis and with the presence of residual amounts of γ-Al_2O_3 in the case of BaIAl14–1470. The surface area is retained up to 1670 K in the case of BaAl12 due to the thermal stability of the Ba–β-Al_2O_3 phase. On the other hand, a further decrease in surface area is observed for both BaIAl14 and BaIAl9.

4. Discussion

Table II summarizes the phase composition of pure Al_2O_3 and of BaIAl14, BaIAl12, and BaIAl9 as a function of calcination temperature. In dried, pure Al_2O_3 sample, the XRD results provide evidence for the presence of crystalline $(NH_4)_2Al_6(OH)_{14}(CO_3)_3 \cdot xH_2O$, while in the case of the barium-containing samples, the same compound is detected together with crystalline mixed Ba–Al compounds, that have been tentatively identified as $BaAl_2(CO_3)_2(OH)_4 \cdot 2H_2O$) and $Ba_2Al_4(OH)_{16}$. The high surface area measured for dried samples, of the order of $\approx 200\ m^2\,g^{-1}$, indicates that amorphous compounds are also present, probably consisting of carbonates, hydroxides and mixed hydroxycarbonates, as suggested by FT–IR data. Chemical analysis confirms that Ba^{2+} and Al^{3+} ions have been quantitatively precipitated. The above results demonstrate that the method of preparation employed in the present work, which makes use of $(NH_4)_2CO_3$ as a precipitating agent, is suitable for the quantitative precipitation of well-dispersed Ba^{2+} and Al^{3+} ions in the form of hydroxycarbonates, hydroxides and possibly carbonates.

All the crystalline phases that are present in the dried precursors easily decompose upon calcination at 470 K to give microcrystalline pseudobohemite, amorphous barium-containing compounds and traces of microcrystalline $BaCO_3$. Accordingly the samples show high surface areas of $\approx 300\ m^2\,g^{-1}$. It is worth noticing that the high values of the surface area result from the small dimensions of the aggregates that are obtained either directly during precipitation in the

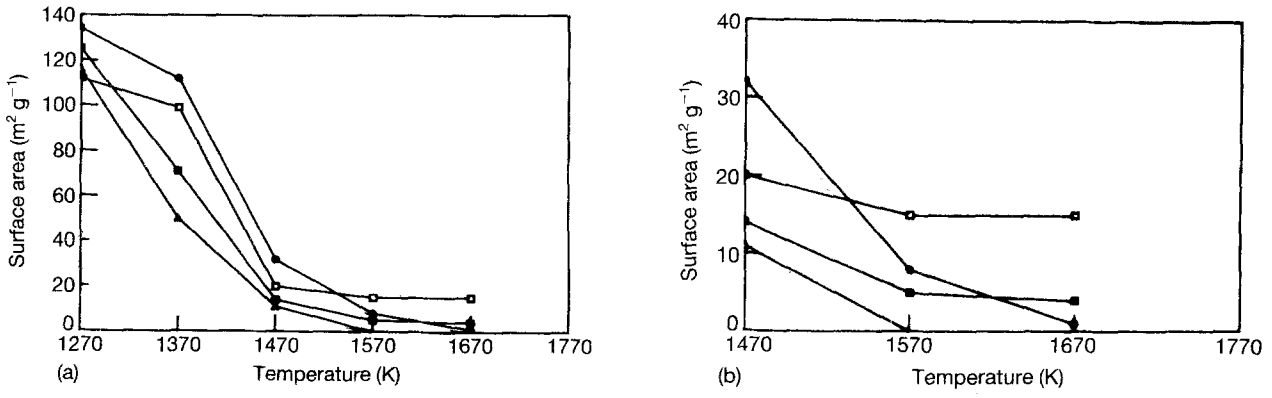

Figure 11 (a) Surface areas of (△) Al_2O_3, (●) BaIAl14, (□) BaIAl12 and (■) BaIAl9 calcined in the temperature range 1270–1670 K. (b) The data in the temperature range 1470–1670 K shown with larger scale.

TABLE II Thermal evolution of Al_2O_3, BaIAl14, BaIAl12 and BaIAl9

T (K)	Al_2O_3	BaIAl14	BaIAl12	BaIAl9
380	$(NH_4)_2Al_6(OH)_{14}(CO_3)_3{\cdot}H_2O$		$(NH_4)_2Al_6(OH)_{14}(CO_3)_3{\cdot}H_2O$, $Ba_2Al_4(OH)_{16}$ and/or $BaAl_2(CO_3)_2(OH)_4{\cdot}H_2O$	
470	Pseudobohemite		Pseudobohemite + CO_3^{2-} species	
770–970	γ-Al_2O_3		γ-Al_2O_3 + CO_3^{2-} species	
1170	θ-Al_2O_3 + γ-Al_2O_3		$BaAl_2O_4$ + CO_3^{2-} species + γ-Al_2O_3	
1270	θ-Al_2O_3		$BaAl_2O_4$ + CO_3^{2-} species + γ-Al_2O_3	
1370	θ-Al_2O_3 + α-Al_2O_3		$BaAl_2O_4$ + Ba–β-Al_2O_3 + CO_3^{2-}species + γ-Al_2O_3	
1470	α-Al_2O_3	Ba–β-Al_2O_3 $BaAl_2O_4$	Ba–β-Al_2O_3 $BaAl_2O_4$	Ba–β-Al_2O_3 $BaAl_2O_4$
1670	α-Al_2O_3	Ba–β_I-Al_2O_3 2% α-Al_2O_3	Ba–$\beta_I\beta_{II}$-Al_2O_3	Ba–β_{II}-Al_2O_3 2% $BaAl_2O_4$

form of amorphous compounds, or by decomposition of thermally unstable crystalline phases. This eventually favours the dispersion of barium that plays a key role in the mechanism of formation of the Ba–β-Al_2O_3 phases as discussed below.

Upon calcination at 770 K the formation of microcrystalline γ-Al_2O_3 from pseudobohemite is observed for all the samples. However, in the case of Ba–Al–O samples, the crystallites of γ-Al_2O_3 are apparently smaller and significant amounts of amorphous carbonates are observed as compared to pure Al_2O_3. The differences between Ba–Al–O and pure Al_2O_3 become more evident when the samples are calcined at higher temperatures. Upon calcination at 1170 K in the case of pure alumina, the incipient γ-$Al_2O_3 \rightarrow \theta$-$Al_2O_3$ phase transition is observed, as expected. This is accompanied by a sintering of the material that results in a decrease of the surface area. In the case of all BaIAlX–1170 samples, the γ-$Al_2O_3 \rightarrow \theta$-$Al_2O_3$ phase transition is not observed and sintering phenomena of the alumina matrix seem non-evident, whereas crystalline $BaAl_2O_4$ forms. Significant amounts of amorphous carbonates are always present.

In Al_2O_3 the γ-$Al_2O_3 \rightarrow \theta$-$Al_2O_3$ phase transition is completed upon calcination at 1270 K and, as a consequence, a further significant decrease in the surface area is manifest (from $\approx 150\ m^2\ g^{-1}$ to $\approx 50\ m^2\ g^{-1}$). On the contrary, none of the Ba–Al–O samples calcined at 1270 K provide evidence for the formation of θ-Al_2O_3, and $BaAl_2O_4$ represents the only well-crystallized phase. Microcrystalline γ-Al_2O_3 and amorphous carbonates are still present. Subsequent calcination at 1370 K of pure Al_2O_3 induces the θ-$Al_2O_3 \rightarrow \alpha$-$Al_2O_3$ transition that is completed at 1470 K. In the case of barium-containing samples, again no alumina transitions are detected; indeed the modulations observed in the XRD spectra can be attributed to microcrystalline γ-Al_2O_3, whereas there is no evidence for the formation of θ-Al_2O_3 and α-Al_2O_3. At 1370 K, the incipient formation of the final Ba–β-Al_2O_3 phase is observed for all the Ba/Al ratios (1/14, 1/12, and 1/9). The surface area of Ba–Al–O samples decreases more slowly, compared to Al_2O_3, in the range 1170–1370 K, in line with the absence of the γ-$Al_2O_3 \rightarrow \theta$-$Al_2O_3 \rightarrow \alpha$-$Al_2O_3$ transitions. This suggests that the surface area of the samples is associated primarily with microcrystalline alumina and is influenced only to a minor extent by the presence of crystalline $BaAl_2O_4$.

It has been reported [21–23] that the presence of small amounts (1%–2% wt/wt) of alkaline metal ions effectively inhibits the sintering and the phase transitions of γ-Al_2O_3 through interaction with surface hydroxyls. The presence of dispersed barium in our samples is provided by quantitative XRD analysis performed at 1170, 1270, 1370 and 1470 K. The analyses show that the amount of $BaAl_2O_4$ accounts for the best of 65% of the overall barium content, even after long calcination times (25 h). Additional evidence for the presence of dispersed barium has been found through the detection of amorphous carbonates in the FT–IR spectra up to 1370 K, that have been tentatively identified as barium carbonate species. Accordingly, the absence of γ-Al_2O_3 transition in barium-containing samples can be associated with the presence of barium dispersed in the alumina matrix, the dispersion being favoured by the small dimension of the aggregates.

Upon calcination at 1470 K in BaIAl14 and BaIAl12 samples, the formation of the Ba–β-Al_2O_3 phase is almost completed and this parallels the depletion of both crystalline $BaAl_2O_4$ and dispersed barium-containing compounds. Indeed, the XRD spectra of these samples show the presence of major amounts of Ba–β-Al_2O_3 with small residual quantities of $BaAl_2O_4$, whereas the characteristic FT–IR bands of carbonate species associated with dispersed barium compounds are no longer observed. The formation of Ba–β-Al_2O_3 phase is more difficult in the case of BaIAl9. Indeed the XRD features of Ba–β-Al_2O_3 phase are evident but large amounts of crystalline $BaAl_2O_4$ are detected and carbonate species are still observed at 1470 K.

The formation of Ba–β-Al_2O_3 phases is completed in all samples upon calcination at higher temperatures (1670 K) and $BaAl_2O_4$ is totally consumed except for BaIAl9. Detailed investigations performed on the samples calcined at 1670 K by means of Rietveld

analysis revealed that traces of α-Al_2O_4 (2%) and $BaAl_2O_4$ (2%) are still present in BaAl14 and BaAl9, respectively, while BaAl12 is monophasic. The structure of the Ba–β-Al_2O_3 phases depends on Al/Ba ratios. In the sample with the lowest barium content (Al/Ba = 14), the barium-poor β_I phase forms, while in the case of the sample with the highest barium content (Al/Ba = 9) the barium-rich β_{II} phase forms, allocating the excess barium ions in the spinel blocks. In the case of the intermediate composition (Al/Ba = 12), a mixed Ba–$\beta_I\beta_{II}$-Al_2O_3 phase forms. This intermediate phase is supposed to be originated by the intergrowth of β_I and β_{II} domains that is favoured by the close similarity between the two structures. It is worth stressing that for all Al/Ba ratios, a characteristic layered structure is obtained that is closely related to the original γ-Al_2O_3 matrix, being constituted by an array of γ-Al_2O_3-type spinel blocks intercalated by barium planes.

Our data show that both $BaAl_2O_4$ and dispersed barium react with γ-Al_2O_3 simultaneously to give Ba–β-Al_2O_3. This eventually suggests that two routes operate in the formation of the Ba–β-Al_2O_3 phase, namely solid-state reactions between γ-Al_2O_3 and dispersed barium compounds and between γ-Al_2O_3 and $BaAl_2O_4$. The inhibiting effect of barium upon sintering and γ-Al_2O_3 phase transitions ensures the presence of aggregates of γ-Al_2O_3 with small dimensions up to the threshold temperature for the formation of Ba–β-Al_2O_3 (1370–1470 K). This eventually favours both reaction routes. Based on the strong structural analogies of γ-Al_2O_3 and Ba–β-Al_2O_3 phase, the formation of Ba–β-Al_2O_3 can probably occur via diffusion of barium ions in γ-Al_2O_3 and the observed threshold temperature for the formation of Ba–β-Al_2O_3 can be associated with the mobility of barium ions within the alumina matrix.

It has been reported in the literature [5] that a Ba–β-Al_2O_3 material with very small surface area is obtained when the sample is prepared by solid-state reaction between powders of γ-Al_2O_3 and $BaCO_3$, due to the occurrence of slow diffusion-controlled solid-state reactions involving $BaAl_2O_4$ as intermediate. The same authors developed a preparation method based on the hydrolysis of alkoxides to ensure interspersion of the constituents within an amorphous organic matrix. This preparation method prevents the formation of $BaAl_2O_4$ as an intermediate and the final material with β-Al_2O_3 structure and high surface area (15 $m^2 g^{-1}$) directly forms from the thermally decomposed precursors. However, our data prove that the formation of well-crystallized $BaAl_2O_4$ as an intermediate does not prevent the synthesis of Ba–β-Al_2O_3 with high surface area (10–15 $m^2 g^{-1}$). It appears, therefore, that the surface area of the final material is controlled by the presence of dispersed barium that prevents sintering and transition of γ-Al_2O_3 and the related irreversible loss of surface area.

The surface area curves in Fig. 11 show that BaAl12 has the maximum resistance to sintering. Indeed, BaAl12 retains a surface area of 10–15 $m^2 g^{-1}$ up 1670 K, while for BaAl14 and BaAl9, a surface area loss is observed to the final values of 2 and 4 $m^2 g^{-1}$, respectively. This behaviour can be associated with the presence of small amounts of well-crystallized α-Al_2O_3 and $BaAl_2O_4$ in BaAl14 and BaAl9 samples and/or with minor structural differences in the Ba–β-Al_2O_3 phase of the three samples. Moreover, in the case of BaAl9 the lower surface area can also be associated with the more difficult formation of the Ba–β-Al_2O_3 [17].

5. Conclusions

1. The present method of preparation, based on the precipitation of the constituents from an aqueous solution of nitrates using $(NH_4)_2CO_3$ as precipitating agent, is suitable for the quantitative precipitation of the ions and leads to a mixture of hydroxycarbonates, hydroxides and carbonates that decompose upon calcination at 470 K. A microcrystalline material with high surface area, with small dimensions of the aggregates and with barium dispersed in the alumina matrix, is obtained.

2. Two routes operate in the formation of Ba–β-Al_2O_3 phases, namely solid-state reaction between γ-Al_2O_3 and dispersed barium and between γ-Al_2O_3 and $BaAl_2O_4$. The formation of the final material probably occurs according to a mechanism common to both routes, via diffusion of barium ions in γ-Al_2O_3. The observed threshold temperature of 1370 K required for the formation of Ba–β-Al_2O_3 phases is probably associated with the mobility of barium ions within the γ-Al_2O_3 matrix.

3. Upon calcination at 1670 K, a monophasic material is obtained in the case of the BaAl12 sample while α-Al_2O_3 and $BaAl_2O_4$ are also present in the case of BaAl14 and BaAl9 samples, respectively. Different Ba–β-Al_2O_3 phases are observed depending on the Al/Ba atomic ratio: for Al/Ba = 9 a barium-rich phase (β_{II}) is obtained, while for Al/Ba = 14 a barium-poor phase (β_I) is detected. In the case of Al/Ba = 12, the structure originates from the intergrowth of β_I and β_{II} phases.

4. The obtainment of the final material with β-Al_2O_3 structure and good morphological properties is not prevented by the formation of $BaAl_2O_4$ as intermediate. Instead it is probably allowed by the presence of barium ions dispersed in the γ-Al_2O_3 matrix, that inhibits sintering and transitions of γ-Al_2O_3, favouring solid-state reaction to give β-Al_2O_3.

Acknowledgement

This study was supported by the CNR-ENEL project "Interaction of Energy Systems with Human Health and Environment", Rome, Italy.

References

1. D. L. TRIMM, *Appl. Catal.* **7** (1983) 249.
2. R. PRASAD, L. A. KENNEDY and E. RUCKENSTEIN, *Catal. Rev. Sci. Eng.* **26** (1984) 1.
3. L. D. PFEFFERLE, W. C. PFEFFERLE, *ibid.* **29** (1987) 219.
4. M. MACHIDA, K. EGUCHI and H. ARAI, *J. Catal.* **103** (1987) 385.

5. *Idem, Bull. Chem. Soc. Jpn* **61** (1988) 3659.
6. E. M. LEVIN, C. R. ROBBINS and H. F. McMURDIE, in "Phase Diagrams for Ceramists", edited by M. K. Reser (The American Ceramic Society, 1985) p. 97.
7. H. ARAI, K. EGUCHI and M. MACHIDA, in "MRS International Meeting on Advanced Materials", Vol. 2 (1989) p. 243.
8. M. MACHIDA, K. EGUCHI and H. ARAI, *J. Catal.* **120** (1989) 377.
9. S. KIMURA, E. BANNAI and I. SHINDO, *Mater. Res. Bull.* **17** (1982) 209.
10. N. IYI, S. TAKEKAWA, Y. BANDO and S. KIMURA, *J. Solid State Chem.* **47** (1983) 34.
11. G. GROPPI, M. BELLOTTO, C. CRISTIANI, P. FORZATTI and P. L. VILLA, *Appl. Catal. A. General*, **104** (1993) 101.
12. H. P. KLUG and L. E. ALEXANDER, in "X-Ray Diffraction Procedures" (Wiley, New York, 1974).
13. J. MIGNOT and D. RONDOT, *Acta Crystallogr.* **A33** (1977) 327.
14. R. F. VOGEL, G. MARCELIN and W. L. KEHL, *Appl. Catal.* **12** (1984) 237.
15. T. ASSIH, A. AYRAL, M. ABENOZA and J. PHALIPPOU, *J. Mater. Sci.* **23** (1988) 3326.
16. A. F. WELLS, in "Structural Inorganic Chemistry" (Clarendon Press, Oxford, 1975) p. 458.
17. M. BELLOTTO, F. ASSANDRI, V. BOLIS, C. CRISTIANI, G. GROPPI and P. FORZATTI, *J. Solid State Chem.*, in press.
18. N. IYI, Z. INOUE, S. TAKEKAWA and S. KIMURA, *J. Solid State Chem.* **60** (1985) 41.
19. *Idem, ibid.* **52** (1984) 66.
20. N. YAMAMOTO and M. O'KEFEE, *Acta Crystallogr.* **B40** (1984) 21.
21. P. BURTIN, J. P. BRUNELLE, M. PIJOLAT and M. SOUSTELLE, *Appl. Catal.* **34** (1987) 225.
22. M. L. F. JOHNSON, *J. Catal.* **123** (1990) 245.
23. A. B. STILES, *Catal. Today* **14** (1992) 269.

Received 6 April
and accepted 10 December 1993